Letter

Pine Island Glacier Ice Shelf (West Antarctica) is more sensitive to climate conditions than to rheological parameters on multidecadal timescales

Olga Sergienko *

Atmospheric and Oceanic Sciences Program, Princeton University, Princeton, New Jersey 08540, USA

(Received 8 March 2025; accepted 12 May 2025; published 10 June 2025)

This article is part of a Physical Review *Collection on the Physics of Changing Climate.*

Antarctic ice shelves, floating extensions of the Antarctic Ice Sheet, regulate the ice discharge from the ice-sheet interior into the surrounding oceans and, as a result, the ice-sheet contribution to the sea level. On a timescale longer than several months, the flow of bodies of ice, such as ice sheets and ice shelves, is controlled by the ice non-Newtonian viscosity and its rheological parameters, i.e., the ice stiffness and the exponent of the rheology power-law functional form. Recent studies suggest that the value of the rheological exponent may be higher than that typically used in studies of ice shelves. It is unclear, however, what effects this difference might have on the behavior of ice shelves in general and particularly on multidecadal timescales. In order to evaluate such effects on the behavior of the Pine Island Glacier Ice Shelf, one of the fastest changing regions in Antarctica, a suite of numerical simulations has been performed. In these simulations, the ice-shelf rheological parameters have been constrained by means of inverse methods using remote-sensing observations. The results show that for the same submarine melting and different rheological parameters, the difference between the ice-shelf states (thickness and speed) is of the order of 5%. In contrast, for the same rheological parameters and different submarine melting, the difference between the ice-shelf states is significantly larger, of the order of 15% for ice speed and 40% for ice thickness. These results suggest that ice shelves have much higher sensitivity to the impacts of climate conditions, such as submarine melting, than to their rheological parameters.

DOI: 10.1103/n3xh-bt95

Introduction. Ice shelves, the floating extensions that fringe the Antarctic Ice Sheet, determine the rate of ice mass transport from the continent to the ocean, via the effect termed buttressing, the impediment of the ice-shelf flow by rock walls of the coastal embayments or ice rises [1–5]. Ice shelves flow due to internal deformation in response to the gravity force. On timescales longer than several months, the glacial ice is treated as a non-Newtonian fluid, whose viscosity has a power-law dependence on the second invariant of the strain-rate tensor. This functional dependence is known as Glen's flow law [6].

Due to the ice density being smaller than the water density, ice shelves float on top of the ocean, forming sub-ice-shelf cavities. At the base of the ice shelves, ice and sea water exchange energy, mass, and salt fluxes; this results in either sub-ice-shelf melting or refreezing. The former removes mass from ice shelves and the latter adds mass to them. Due to the gravity-driven nature, the ice flow depends on changes in its mass. The rate of flow of ice and its internal deformation are strong functions of the ice rheological parameters. Consequently, changes in both the ice shelf mass due to submarine melting or refreezing and the ice rheological properties impact the flow of ice shelves, which in turn affects the stress regime of the ice shelves and as a result their buttressing on the grounded ice upstream of the grounding lines, the locations where ice loses its contact with the bedrock and starts to float, forming ice shelves [5].

Laboratory experiments suggest that the flow-law exponent, typically denoted by n, is around 2 if ice is deformed under low stresses and around 4 if it is deformed under large stresses [7]. *In situ* measurements by means of various techniques [8,9] suggest values between 3 and 5. However, such measurements are very sparse due to logistical and technological difficulties. Ice-flow models ranging from idealized one dimensional [10] to continental scale [11] use the value of $n = 3$. Recent analysis of satellite observations of the Antarctic ice shelves' flow suggests that $n \approx 4$ [12].

One of the glaciers experiencing significant mass loss is Pine Island Glacier located in the Amundsen Sea Embayment, West Antarctica [Fig. 1(a)]. The Pine Island Glacier Ice Shelf (PIGIS) is subject to strong submarine melting because it is in contact with warm Circumpolar Deep Water [17,18]. The existing studies focused on either the PIGIS present-day behavior or projections of its future behavior under warming climate conditions use the flow-law exponent $n = 3$ [19,20]. It is unclear, however, what effects different values of n may have on the PIGIS flow and its temporal evolution. To quantify the relative effects of its rheological parameters and submarine melting on multidecadal timescales, this study uses a combination of remote sensing observations, inverse methods, and numerical models. The observed state [21,22] and inversion techniques [23] are used to infer its rheological parameters. These parameters are used in two sets of numerical simulations of the PIGIS evolution run for 100 years. The first set of simulations uses the submarine melting rates inferred from remote sensing observations [24]; the second set uses a prescribed value of submarine melting rates. The results

*Contact author: osergien@princeton.edu

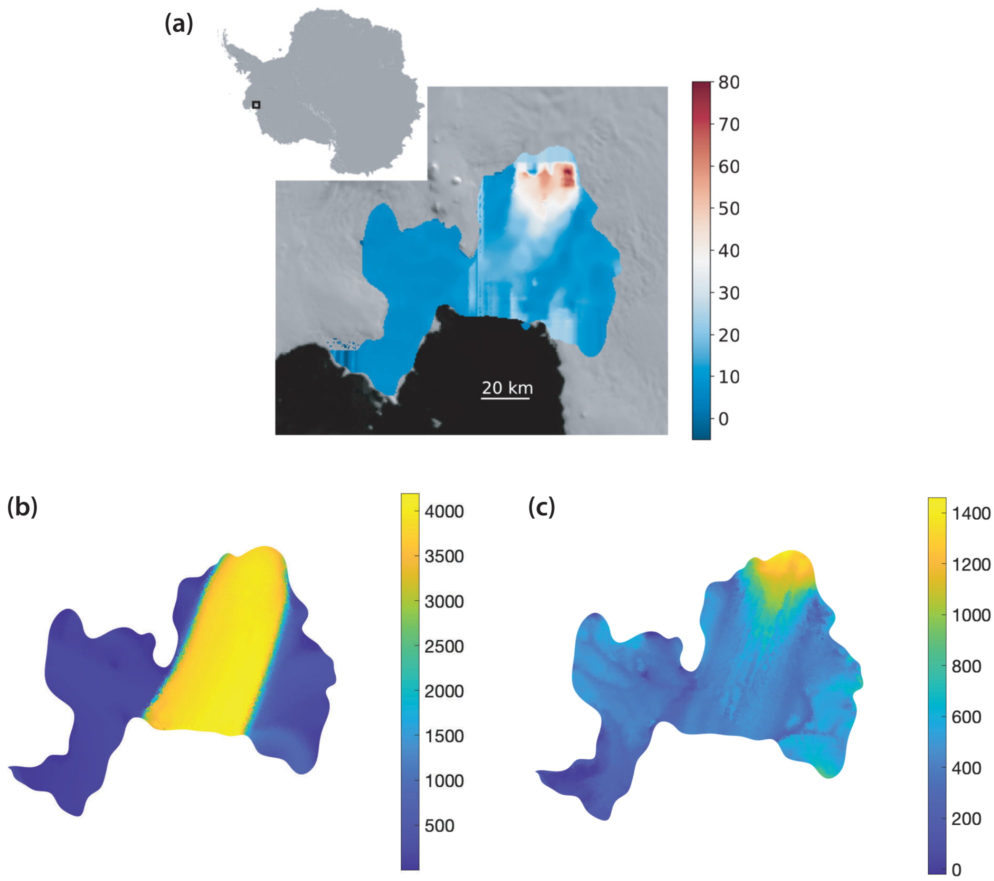

FIG. 1. Pine Island Glacier Tongue. (a) Sub-ice-shelf melt rate (m yr^{-1}) [13]. The background and inset are MODIS Mosaic of Antarctica [14]; a black rectangle in the inset map shows the location of the image. (b) Ice speed (m yr^{-1}) [15]. (c) Ice thickness (m) [16].

suggest that on these timescales, the PIGIS flow is more sensitive to the submarine melting distribution than to the details of the rheological parameters, as long as these parameters are constrained by observations.

Inference of the rheological parameters from observations. The gravity-driven flow of large bodies of ice can be treated as Stokes flow. Under approximations appropriate to ice shelves, e.g., negligible vertical shear, their flow can be described by the vertically integrated momentum balance [25]

$$[2\nu H(2u_x + v_y)]_x + [\nu H(u_y + v_x)]_y = \rho g' H H_x, \quad (1a)$$

$$[\nu H(u_y + v_x)]_x + [2\nu H(u_x + 2v_y)]_y = \rho g' H H_y, \quad (1b)$$

where H is the ice-shelf thickness, u and v are vertically averaged ice velocity components, and g' is the reduced gravity defined as $g' = \delta g$, with $\delta = \frac{\rho_w - \rho}{\rho_w}$, $\rho_w = 1027$ km m^{-3} the sea-water density, and $\rho = 917$ km m^{-3} the ice density. The subscripts indicate partial derivatives with respect to the horizontal coordinates. The ice viscosity ν is described by a shear-thinning power-law rheology

$$\nu = \frac{\bar{B}}{2}\dot{e}_{II}^{(1-n)/2n} = \frac{\bar{B}}{2}\left(u_x^2 + v_y^2 + \frac{1}{4}(u_y + v_x)^2 + u_x v_y\right)^{(1-n)/2n}, \quad (2)$$

where $\bar{B}$ is a vertically averaged ice-stiffness parameter and $\dot{e}_{II}$ is the second invariant of the strain-rate tensor. The momentum balance (1) and the second equality of Eq. (2) take into account the ice incompressibility, i.e.,

$$u_x + v_y + w_z = 0, \quad (3)$$

where w is the vertical velocity component.

In contrast to laboratory settings where rheological parameters of ice samples can be measure directly, such measurements cannot be performed on the scales of ice sheets or ice shelves. In past decades, indirect methods have been developed to infer these parameters from remote sensing observations using inversion techniques [23]. Here the PIGIS rheological parameters have been inferred by means of a control method from the ice velocities derived from satellite-borne interferometric synthetic aperture radar observations [15] [Fig. 1(b)] and airborne measurements of the ice thickness H [16] [Fig. 1(c)]. In this method, a cost function, defined as a misfit between the observed ice velocities and computed with Eqs. (1) and (2) using observed values of the ice thickness, is minimized with respect to the control parameter $\bar{B}$. The inversions are performed using a finite-element solver COMSOL [26], which has been used in studies of inversions of glaciological parameters [27,28], in studies of ice-shelf flow [5,29,30], and in other glaciological applications [31–33]. Details of the inversion procedures are described in the Supplemental Material [34] (Sec. I).

The inferred spatial distributions of $\bar{B}$ obtained using spatially uniform values $n = 3$ and 4 are shown in Fig. 2. A common characteristic of $\bar{B}$ for both values of n is its low

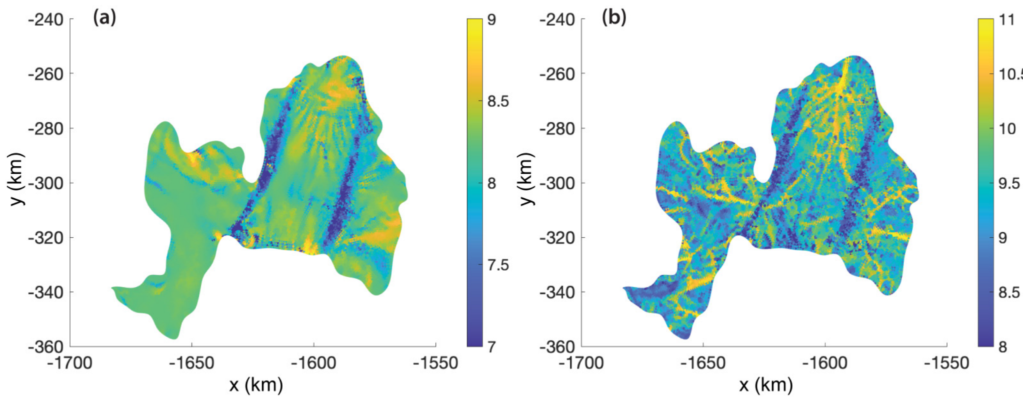

FIG. 2. Inferred ice-stiffness parameter $\bar{B}$ (the color bar shows $\log_{10}\bar{B}$) for (a) $n = 3$ and (b) $n = 4$.

values along the shear margins, the narrow boundary layers where ice flow experiences large gradients [Fig. 1(b)] and, as a result, high strain rates. The regions with large values of $\bar{B}$ correspond to the locations of melt channels, morphological forms, several hundreds of meters high and a few kilometers wide, observed on the ice-shelf base [35,36] and formed as a result of tightly coupled interactions between submarine melting, the ice-shelf flow, and the ocean circulation in the sub-ice-shelf cavity [29]. These channels are characterized by large variations of the ice thickness [35,36], and these variations are a likely cause of large variations of the vertically averaged ice-stiffness parameter. For $n = 4$ high values of $\bar{B}$ are more spatially confined within the channels [Fig. 2(b)] compared to values of $\bar{B}$ inferred with $n = 3$ [Fig. 2(a)].

Although it is possible to simultaneously infer the spatially heterogeneous ice-stiffness parameter $\bar{B}$ and the spatially heterogeneous flow-low exponent n, the inferred distributions are not unique and, as Fig. 3 illustrates, it is possible to obtain more than one combination of spatial distributions of these parameters (details are in the Supplemental Material [34], Sec. I). Similar to the inversions with constant values of n (Fig. 2), the shear margins are distinct features in the inferred patterns, and the flow-law exponent n has larger values there [Fig. 3(a)]. However, the values of $\bar{B}$ obtained in the same inversion [Fig. 3(c)] are not as low as in another inversion [Fig. 3(d)], in which shear margins are less pronounced in n [Fig. 3(b)]. This spatial distribution of n is characterized by low values of n at the locations of melt channels. Its magnitude varies from approximately 2.5 to approximately 4.

The inversion results suggest that the locations where either ice flow (shear margins) or ice thickness (melt channels) experience large variations are characterized by large variations in the inferred rheological parameters. A comparison of the inferred distributions with constant and spatially variable values of n suggests that at the locations with lower values of $\bar{B}$ (shear margins), values of n are larger [Fig. 3(a)]. Conversely, at the locations with larger values of $\bar{B}$ (melt channels), values of n are lower [Fig. 3(b)].

Impacts of rheological parameters and submarine melting on the temporal evolution of the Pine Island Glacier Ice Shelf. In order to assess the PIGIS relative sensitivity to its rheological parameters and submarine melting, two sets of numerical experiments have been performed. In these simulations, the momentum balance (1) and the mass balance

$$H_t + H(u_x + v_y) + uH_x + vH_y = -\dot{b} \qquad (4)$$

are solved simultaneously. In Eq. (4), $\dot{b}$ is the submarine melt rate. In the performed simulations, the ice viscosity (2) is computed using the inferred rheological parameters (Figs. 2 and 3). The ice-shelf surface accumulation rate (negative for ablation) is assumed to be smaller than the submarine melt rate $\dot{b}$. Because these simulations aim to evaluate the PIGIS sensitivity, as opposed to projecting its future state, the submarine melt rate distribution is kept constant in time. For the same reason, neglecting the surface accumulation rate in (4) does not affect the drawn conclusions. As discussed in the preceding section, the inferred rheological parameters are colocated with the shear margins and melt channels. Both are persistent features; therefore, their impacts on the rheological parameters are persistent as well. For this reason, the spatial distributions of the inferred ice stiffness and the power-law exponents are kept the same in the course of simulations. The observed values of the ice velocities and thickness are used as the boundary conditions at the grounding line. At the calving front, i.e., the ice-shelf seaward boundary, the boundary condition is on the vertically integrated stress; it is balanced by the vertically integrated hydrostatic pressure in the ocean.

Two sets of simulations ran for 100 years. In the first set, the submarine melt rate $\dot{b}$ was derived from satellite observations [Fig. 1(a)] [24]. The second set used a constant value $\dot{b} = 0.3$ m yr^{-1}. With this value, the ice-shelf thickness remained positive through the course of simulations. Using the area-averaged value of the observationally derived values of $\dot{b}$ [Fig. 1(a)] of 5.66 m yr^{-1} led to a rapid melt through of thin parts of the PIGIS. As in preceding section, numerical simulations have been performed with the finite-element solver COMSOL [26]. The details are described in the Supplemental Material [34] (Sec. II).

The results of the first set of simulations are summarized in Fig. 4. Figures 4(a) and 4(e) show the ice speed and thickness simulated with the inferred ice-stiffness parameter for $n = 3$ [Fig. 2(a)] at the end of 100-yr simulations. These fields are used as references, and the results of other simulations are reported as deviations from them. Figures 4(b)–4(d) show the relative deviations (in percent) of the speed and

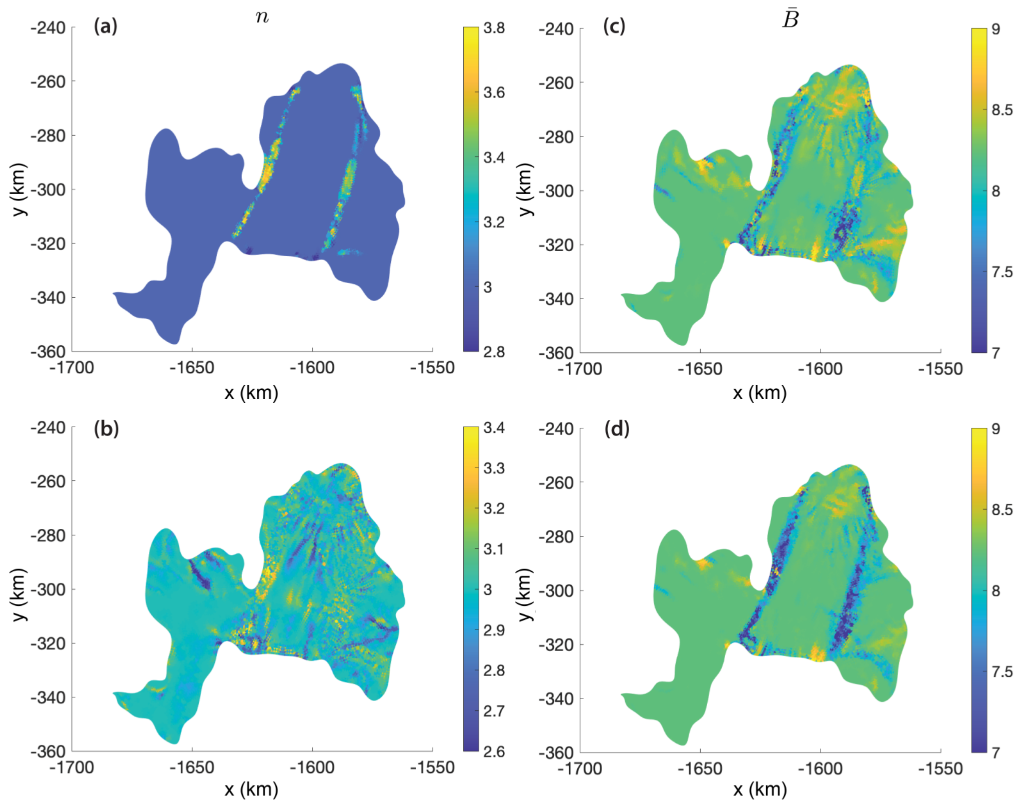

FIG. 3. Inferred rheological parameters: (a) and (b) exponent n and (c) and (d) ice stiffness parameter $\log_{10}\bar{B}$.

Figs. 4(f)–4(h) show the relative deviations (in percent) of the ice thickness. The rows correspond to various rheological parameters: Figs. 4(b) and 4(f) correspond to the inferred $\bar{B}$ with $n = 4$ [Fig. 2(b)]; the third and fourth rows correspond to the inferred $\bar{B}$ with spatially variable values of n shown in Fig. 3 [the third row corresponds to Figs. 3(a) and 3(b), the fourth to Figs. 3(c) and 3(d)]. The spatial patterns of the relative deviations are different for different rheological parameters. In the case of $n = 4$ [Figs. 4(b) and 4(f)], the ice speed is higher [Fig. 4(b)] and the ice thickness is smaller [Fig. 4(f)] in the ice-shelf central part and near the calving front. For the case of the heterogeneous n the spatial patterns are reversed. For n and $\bar{B}$ shown in Figs. 3(a) and 3(c) [Figs. 4(c) and 4(g)], the flow is slightly faster and the ice is slightly thinner in the center of the trunk [Figs. 4(c) and 4(g)]. For n and $\bar{B}$ shown in Figs. 3(b) and 3(d) [Figs. 4(d) and 4(h)], the flow is slightly slower and the ice is slightly thicker in the trunk [Figs. 4(d) and 4(h)]. However, for all different combinations of the rheological parameters, the deviations of the ice flow and thickness are within 5% of their values simulated with the typical value $n = 3$ and the corresponding $\bar{B}$ [Fig. 2(a)].

In order to assess how the magnitudes of the effects of the rheological parameters compare to the effects of the submarine melt rate, the second set of 100-yr simulations has been run with a constant value of $\dot{b} = 0.3$ m yr^{-1}. Figure 5 illustrates the effects of the submarine melt rate on the ice-shelf state simulated with different rheological parameters. Figures 5(a) and 5(e) correspond to $n = 3$ and $\bar{B}$ shown in Fig. 2(a), Figs. 5(b) and 5(f) correspond to $n = 4$ and $\bar{B}$ shown in Fig. 2(b), Figs. 5(c) and 5(g) correspond to a combination of n and $\bar{B}$ and shown in Figs. 3(a) and 3(c), and Figs. 5(d) and 5(h) correspond to a combination of $\bar{B}$ and n shown in Figs. 3(b) and 3(d). The panels show the relative difference between simulations with the observationally derived values of submarine melting $\dot{b}$ shown in Fig. 1(a) and with the constant value of $\dot{b}$. For all rheological parameters, the differences between simulations with spatially variable submarine melt rates are of the order of 15% for the ice flow [Figs. 5(a)–5(d)] and 40% for the ice thickness [Figs. 5(e)–5(h)]. These deviations are substantially larger than those obtained in the first set of simulations. Hence, these results suggest that for the PIGIS, the impacts of the submarine melting are substantially stronger than the impacts of its rheological parameters.

Discussion. Applications of the inverse methods to the PIGIS show that its ice-stiffness parameters inferred from the present-day observations assuming constant values of the flow-law exponent $n = 3$ and 4 have similar spatial patterns. The ice stiffness has low values along the shear margins and large values in the areas of the observed melt channels. Simultaneous inversions of the ice-stiffness parameter and the flow-law exponent result in a manifold of spatially heterogeneous fields. These combinations of spatial distributions of the ice-stiffness parameter and the flow-law exponent yield computed ice speeds that fit the observed values equally well. The existence of multiple spatial distributions of the inferred rheological parameters is due to the ill-posedness of the inverse problem and nonuniqueness of its solutions. Additional observational constraints, e.g., the ice temperature distribution and ice fabric, are required to determine the most likely combination of these parameters.

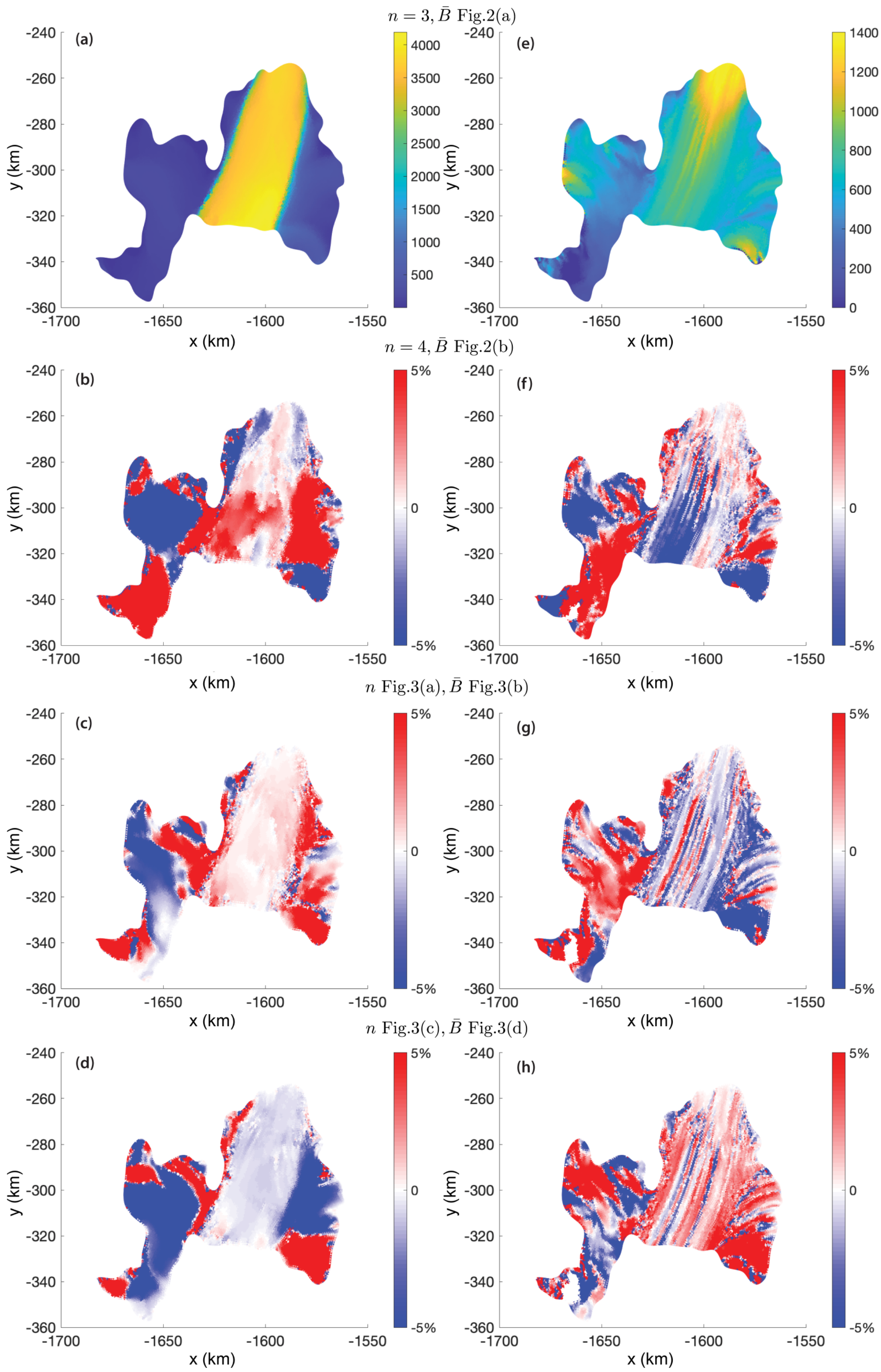

FIG. 4. Effects of rheological parameters on the ice-shelf speed and ice thickness at the end of 100-yr simulations with the observationally derived melt rate [Fig. 1(a)]. (a) Ice velocity $V_{n=3}$ and (e) ice thickness $H_{n=3}$ computed with $n = 3$ and $\bar{B}$ shown in Fig. 2(a). (b)–(d) and (f)–(h) Relative deviations of the ice speed and thickness computed with other values of n and $\bar{B}$ [shown in Figs. 2(b) and 3]. (b)–(d) $\Delta V = \frac{V - V_{n=3}}{V_{n=3}}$ and (f)–(h) $\Delta H = \frac{H - H_{n=3}}{H_{n=3}}$, where V and H are the ice speed and thickness computed with the respective values of the rheological parameters.

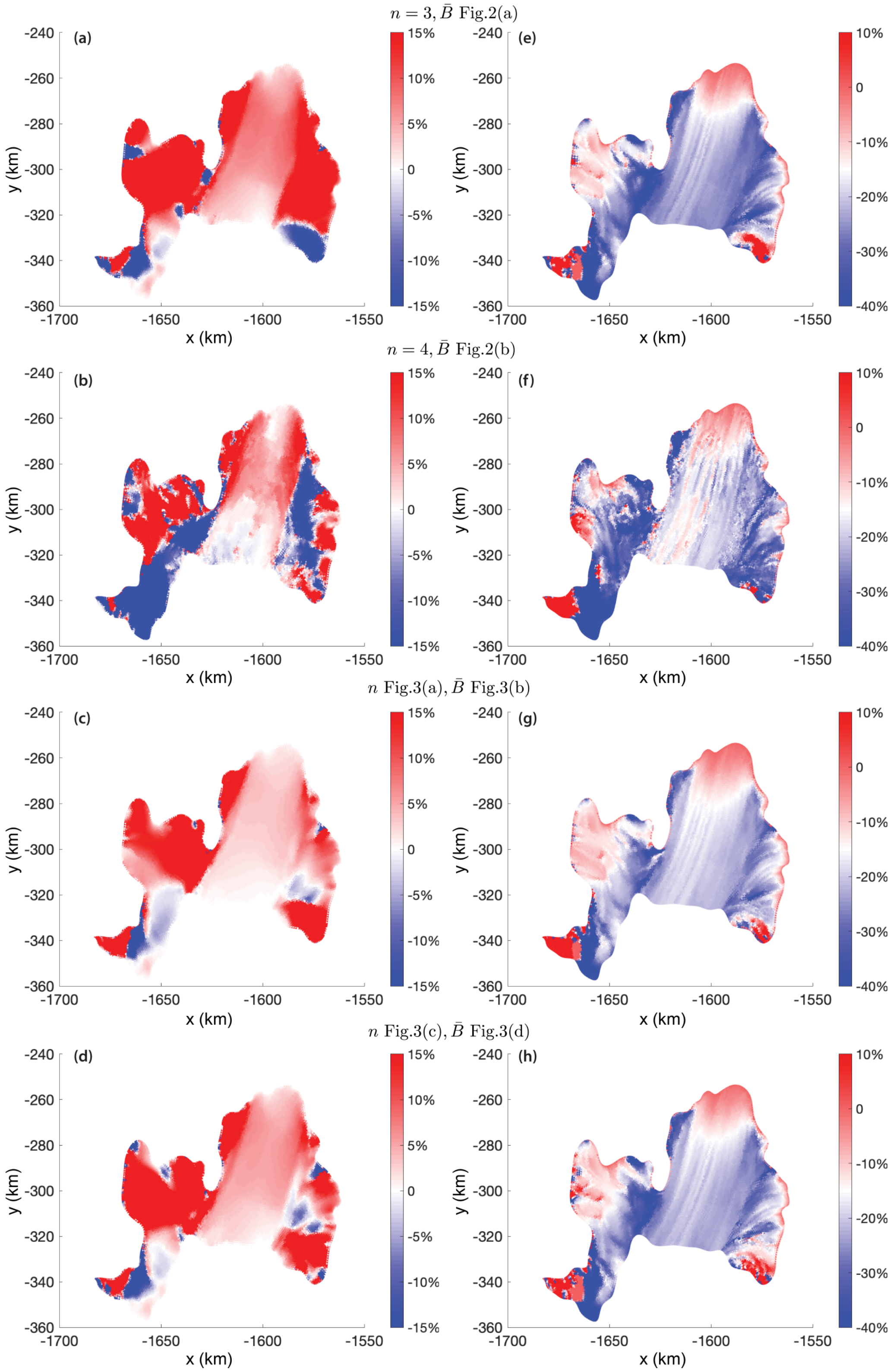

FIG. 5. Effects of submarine melting on the ice-shelf speed and ice thickness at the end of 100-yr simulations for (a)–(d) $\Delta V = \frac{V - V_{\dot{b}=\mathrm{const}}}{V_{\dot{b}=\mathrm{const}}}$ and (e)–(h) $\Delta H = \frac{H - H_{\dot{b}=\mathrm{const}}}{H_{\dot{b}=\mathrm{const}}}$, where V and H are ice speed and thickness computed with the observationally derived melt rate [Fig. 1(a)] and $V_{\dot{b}=\mathrm{const}}$ and $H_{\dot{b}=\mathrm{const}}$ computed with a constant melt rate $\dot{b} = 0.3$ m yr^{-1} using the same values of the rheological parameters.

Results of 100-yr simulations that use the inferred rheological parameters and observationally derived or constant melt rates suggest that the PIGIS is more sensitive to the details of submarine melting than to the details of spatial distributions of its rheological parameters. This result can be understood from the following considerations. The rheological parameters and basal melting play different roles in the evolution of the ice-shelf thickness (or mass) and its gravity-driven flow. The rheological parameters affect the ice deformation [the second term on the left-hand side of (4)] and advection [the third and fourth terms on the left-hand side of (4)]. These processes control the redistribution of the ice-shelf mass. In contrast, submarine melting affects the ice loss, i.e., the ice mass itself. Consequently, the detailed knowledge of the submarine melting is crucial for accurate simulation of the ice-shelf state (flow and thickness). If the net effects of the rheological parameters (ice stiffness and the flow-law exponent) can be constrained by observations, as done in this study, the details of their distributions are not as critical to the ice-shelf state as the details of the mass loss due to submarine melting. These results hold for the ice shelves, the floating margins of the ice sheets. The dynamics of the ice flow over the bedrock is fundamentally different from the dynamics of ice shelves, and the detailed knowledge of the ice rheological parameters is crucial for the grounded ice sheets.

Conclusion. Using inverse method techniques, remote sensing observations and numerical modeling, this study has assessed sensitivity of the Pine Island Glacier Ice Shelf (Amundsen Sea Embayment, West Antarctica) to its rheological parameters and climate conditions such as submarine melting. The results show that it is more sensitive to the latter than to the details of the former. These results emphasize the need to improve our understanding of the ice-ocean interactions. This requires developing direct observational methods, theories, and numerical models capable of accurately simulating these interactions and their feedback. Such improvements will allow us to reduce uncertainties in the projections of the ice-sheet contributions to the sea level under changing climate conditions.

Acknowledgments. I would like to thank Editors and an anonymous referee for their useful comments. This study was supported by an Award No. NA23OAR4320198 from the National Oceanic and Atmospheric Administration, U.S. Department of Commerce. The statements, findings, conclusions, and recommendations are those of the author and do not necessarily reflect the views of the National Oceanic and Atmospheric Administration, or the U.S. Department of Commerce.

Data availability. The data that support the findings of this article are openly available [37]; embargo periods may apply.

[1] R. H. Thomas, The creep of ice shelves theory, J. Glaciol. **12**, 45 (1973).

[2] M. Haseloff and O. V. Sergienko, The effect of buttressing on grounding line dynamics, J. Glaciol. **64**, 417 (2018).

[3] M. Haseloff and O. V. Sergienko, Effects of calving and submarine melting on steady states and stability of buttressed marine ice sheets, J. Glaciol. **68**, 1149 (2022).

[4] O. Sergienko and M. Haseloff, 'Stable' and 'unstable' are not useful descriptions of marine ice sheets in the Earth's climate system, J. Glaciol. **69**, 1483 (2023).

[5] O. Sergienko, Treatment of the ice-shelf backpressure and buttressing in two horizontal dimensions, J. Glaciol. **71**, e7 (2025).

[6] J. W. Glen, Experiments on the deformation of ice, J. Glaciol. **2**, 111 (1952).

[7] D. L. Goldsby and D. L. Kohlstedt, Superplastic deformation of ice: Experimental observations, J. Geophys. Res.: Solid Earth **106**, 11017 (2001).

[8] J. F. Nye and N. F. Mott, The flow law of ice from measurements in glacier tunnels, laboratory experiments and the Jungfraufirn borehole experiment, Proc. R. Soc. London A **219**, 477 (1953).

[9] F. Gillet-Chaulet, R. C. A. Hindmarsh, H. F. J. Corr, E. C. King, and A. Jenkins, *In-situ* quantification of ice rheology and direct measurement of the Raymond Effect at Summit, Greenland using a phase-sensitive radar, Geophys. Res. Lett. **38**, L24503 (2011).

[10] J. F. Nye, The mechanics of glacier flow, J. Glaciol. **2**, 82 (1952).

[11] H. Seroussi, S. Nowicki, A. J. Payne, H. Goelzer, W. H. Lipscomb, A. Abe-Ouchi, C. Agosta, T. Albrecht, X. Asay-Davis, A. Barthel, R. Calov, R. Cullather, C. Dumas, B. K. Galton-Fenzi, R. Gladstone, N. R. Golledge, J. M. Gregory, R. Greve, T. Hattermann, and M. J. Hoffman *et al.*, ISMIP6 Antarctica: A multi-model ensemble of the Antarctic ice sheet evolution over the 21st century, Cryosphere **14**, 3033 (2020).

[12] J. D. Millstein, B. M. Minchew, and S. S. Pegler, Ice viscosity is more sensitive to stress than commonly assumed, Commun. Earth Environ. **3**, 57 (2022).

[13] S. Adusumilli, H. A. Fricker, B. Medley, L. Padman, and M. R. Siegfried, *Data from Interannual Variations in Meltwater Input to the Southern Ocean from Antarctic Ice Shelves* (UC San Diego Library Digital Collections, 2020).

[14] T. Haran, J. Bohlander, T. Scambos, T. Painter, and M. Fahnestock, MODIS Mosaic of Antarctica 2008-2009 (MOA2009) Image Map (National Snow and Ice Data Center, Boulder, 2014), Version 1.

[15] E. Rignot, J. Mouginot, and B. Scheuchl., MEaSUREs InSAR-Based Antarctica Ice Velocity Map (National Snow and Ice Data Center, Boulder, 2017), Version 2.

[16] M. Morlighem, MEaSUREs BedMachine Antarctica (National Snow and Ice Data Center, Boulder, 2020), Version 2.

[17] S. S. Jacobs, A. Jenkins, C. F. Giulivi, and P. Dutrieux, Stronger ocean circulation and increased melting under Pine Island Glacier ice shelf, Nat. Geosci. **4**, 519 (2011).

[18] A. Jenkins, D. Shoosmith, P. Dutrieux, S. Jacobs, T. W. Kim, S. H. Lee, H. K. Ha, and S. Stammerjohn, West antarctic ice sheet retreat in the Amundsen Sea driven by decadal oceanic variability, Nat. Geosci. **11**, 733 (2018).

[19] R. M. Gladstone, V. Lee, J. Rougier, A. J. Payne, H. Hellmer, A. Le Brocq, A. Shepherd, T. L. Edwards, J. Gregory, and S. L. Cornford, Calibrated prediction of Pine Island Glacier retreat during the 21st and 22nd centuries with a coupled flowline model, Earth Planet. Sci. Lett. **333–334**, 191 (2012).

[20] H. Seroussi, M. Morlighem, E. Rignot, J. Mouginot, E. Larour, M. Schodlok, and A. Khazendar, Sensitivity of the dynamics of Pine Island Glacier, West Antarctica, to climate forcing for the next 50 years, Cryosphere **8**, 1699 (2014).
[21] J. Mouginot, B. Scheuchl, and E. Rignot, Mapping of ice motion in antarctica using synthetic-aperture radar data, Remote Sens. **4**, 2753 (2012).
[22] M. Morlighem, E. Rignot, T. Binder, D. Blankenship, R. Drews, G. Eagles, O. Eisen, F. Ferraccioli, R. Forsberg, P. Fretwell, V. Goel, J. S. Greenbaum, H. Gudmundsson, J. Guo, V. Helm, C. Hofstede, I. Howat, A. Humbert, W. Jokat, N. B. Karlsson *et al.*, Deep glacial troughs and stabilizing ridges unveiled beneath the margins of the Antarctic ice sheet, Nat. Geosci. **13**, 132 (2020).
[23] V. Rommelaere and D. R. MacAyeal, Large-scale rheology of the Ross Ice Shelf, Antarctica, computed by a control method, Ann. Glaciol. **24**, 43 (1997).
[24] S. Adusumilli, H. A. Fricker, B. Medley, L. Padman, and M. R. Siegfried, Interannual variations in meltwater input to the Southern Ocean from Antarctic ice shelves, Nat. Geosci. **13**, 616 (2020).
[25] D. R. MacAyeal, Large-scale ice flow over a viscous basal sediment: Theory and application to Ice Stream B, Antarctica, J. Geophys. Res. **94**, 4071 (1989).
[26] COMSOL, *Reference Manual* (COMSOL, Boston, 2024).
[27] O. Sergienko and R. C. A. Hindmarsh, Regular patterns in frictional resistance of ice-stream beds seen by surface data inversion, Science **342**, 1086 (2013).
[28] O. Sergienko, T. T. Creyts, and R. C. A. Hindmarsh, Similarity of organized patterns in driving and basal stresses of Antarctic and Greenland ice sheets beneath extensive areas of basal sliding, Geophys. Res. Lett. **41**, 3925 (2014).
[29] O. Sergienko, Basal channels on ice shelves, J. Geophys. Res.: Earth Surf. **118**, 1342 (2013).
[30] D. R. MacAyeal, O. V. Sergienko, A. F. Banwell, G. J. Macdonald, I. C. Willis, and L. A. Stevens, Treatment of ice-shelf evolution combining flow and flexure, J. Glaciol. **67**, 885 (2021).
[31] O. Sergienko, No general stability conditions for marine ice-sheet grounding lines in the presence of feedbacks, Nat. Commun. **13**, 2265 (2022).
[32] O. Sergienko, Marine outlet glacier dynamics, steady states and steady-state stability, J. Glaciol. **68**, 946 (2022).
[33] O. Sergienko and D. J. Wingham, Diverse behaviors of marine ice sheets in response to temporal variability of the atmospheric and basal conditions, J. Glaciol. **70**, e52 (2024).
[34] See Suppemental Material at http://link.aps.org/supplemental/10.1103/n3xh-bt95 for details of the inversion methods and numerical simulations.
[35] D. G. Vaughan, H. F. J. Corr, R. A. Bindschadler, P. Dutrieux, G. H. Gudmundsson, T. N. A. Jenkins, P. Vornberger, and D. J. Wingham, Subglacial melt channels and fracture in the floating part of Pine Island Glacier, Antarctica, J. Geophys. Res.: Earth Surf. **117**, F03012 (2012).
[36] T. P. Stanton, W. J. Shaw, M. Truffer, H. F. J. Corr, L. E. Peers, K. L. Riverman, R. Bindschadler, D. M. Holland, and S. Anandakrishnan, Channelized ice melting in the ocean boundary layer beneath pine Island Glacier, Antarctica, Science **341**, 1236 (2013).
[37] https://zenodo.org/records/5907913.